Measuring line tension: Thermodynamic integration during detachment of a molecular dynamics droplet

Minori Shintaku ; Haruki Oga ; Hiroki Kusudo ; Edward R. Smith ; Takeshi Omori ;
Yasutaka Yamaguchi ✉

Check for updates

CHORUS

View Online

Export Citation

Articles You May Be Interested In

Equilibrium molecular dynamics evaluation of the solid–liquid friction coefficient: Role of timescales

J. Chem. Phys. (July 2023)

Mechanism of surface freezing of alkanes

J. Chem. Phys. (December 2020)

Pinch-off dynamics of an electrohydrodynamic tip streaming jet transforming into the microdroplet

Physics of Fluids (July 2024)
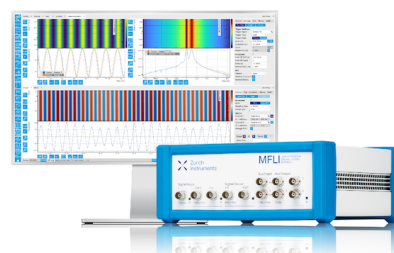
Measuring line tension: Thermodynamic integration during detachment of a molecular dynamics droplet

View Online Export Citation CrossMark

Minori Shintaku,[1] (ID) Haruki Oga,[1,a)] (ID) Hiroki Kusudo,[2,b)] (ID) Edward R. Smith,[3,c)] (ID) Takeshi Omori,[4,d)] (ID) and Yasutaka Yamaguchi[1,5,e)] (ID)

AFFILIATIONS

[1] Department of Mechanical Engineering, Osaka University, 2-1 Yamadaoka, Suita 565-0871, Japan
[2] Department of Mechanical Systems Engineering, Tohoku University, 6-6-01 Aramaki, Aoba-ku, Sendai 980-8579, Japan
[3] Department of Mechanical and Aerospace Engineering, Brunel University London, Uxbridge UB8 3PH, United Kingdom
[4] Department of Mechanical Engineering, Osaka Metropolitan University, 3-3-138 Sugimoto, Sumiyoshi, Osaka 558-8585, Japan
[5] Water Frontier Research Center (WaTUS), Research Institute for Science and Technology, Tokyo University of Science,
 1-3 Kagurazaka, Shinjuku-ku, Tokyo 162-8601, Japan

[a)] Electronic mail: haruki@nnfm.mech.eng.osaka-u.ac.jp
[b)] Electronic mail: kusudo@tohoku.ac.jp
[c)] Electronic mail: Edward.Smith@brunel.ac.uk
[d)] Electronic mail: t.omori@omu.ac.jp
[e)] Author to whom correspondence should be addressed: yamaguchi@mech.eng.osaka-u.ac.jp

ABSTRACT

The contact line (CL) is where solid, liquid, and vapor phases meet, and Young's equation describes the macroscopic force balance of the interfacial tensions between these three phases. These interfacial tensions are related to the nanoscale stress inhomogeneity appearing around the interface, and for curved CLs, e.g., a three-dimensional droplet, another force known as the line tension must be included in Young's equation. The line tension has units of force, acting parallel to the CL, and is required to incorporate the extra stress inhomogeneity around the CL into the force balance. Considering this feature, Bey *et al.* [J. Chem. Phys. **152**, 094707 (2020)] reported a mechanical approach to extract the value of line tension τ_ℓ from molecular dynamics (MD) simulations. In this study, we show a novel thermodynamics interpretation of the line tension as the free energy per CL length, and based on this interpretation, through MD simulations of a quasi-static detachment process of a quasi-two-dimensional droplet from a solid surface, we obtained the value τ_ℓ as a function of the contact angle. The simulation scheme is considered to be an extension of a thermodynamic integration method, previously used to calculate the solid–liquid and solid–vapor interfacial tensions through a detachment process, extended here to the three-phase system. The obtained value agreed well with the result by Bey *et al.* and showed the validity of thermodynamic integration at the three-phase interface.

I. INTRODUCTION

Wetting plays a key role in the behavior of a liquid, especially at the nanoscale where the surface–volume ratio is large. In 1805, Young[1] proposed the following equation as the force balance exerted on the contact line (CL) of a liquid in its vapor atmosphere on a flat solid surface:

$$\gamma_{SL} - \gamma_{SV} + \gamma_{LV} \cos \theta_{CL} = 0, \qquad (1)$$

where γ_{SL}, γ_{SV}, and γ_{LV} are the solid–liquid (SL), solid–vapor (SV), and liquid–vapor (LV) interfacial tensions, respectively, and θ_{CL} denotes the contact angle (CA). Equation (1) is called Young's equation, and the CA is used as a measure of wettability because it can be easily measured experimentally. Note that Young's original work

21 October 2024 15:20:43

considered the mechanical balance lateral to the solid surface and could not possibly be thermodynamic as it was not invented in 1805.[2]

In the latter half of the 19th century, Gibbs and van der Waals formulated surface tension in the framework of thermodynamics, which is sometimes called quasi-thermodynamics because it includes the description of interfaces in addition to bulk.[3–6] In this extended thermodynamic framework, Gibbs formulated surface tension as an excess free energy per unit area of the interface through the definition of the dividing surface. He also introduced the concept of line tension, which we express by τ_ℓ here as an excess free energy per unit length of the CL, i.e., the force tangential to the CL. Boruvka and Neumann[7] included the effect of line tension into Young's equation through the derivation of the variational problem of the equilibrium interface shape as

$$\gamma_{SL} - \gamma_{SV} + \gamma_{LV}\, \cos\,\theta_{LT} + \tau_\ell\kappa = 0, \qquad (2)$$

where θ_{LT} is the CA and κ denotes the (principal) curvature of the CL, e.g., $\kappa = 1/r$ for a three-dimensional axisymmetric cap-shaped hemispherical droplet on a flat solid surface with a circular CL of radius r shown in Fig. 1(b). It follows for Eq. (2) that

$$\cos\,\theta_{LT} = -\frac{\tau_\ell}{\gamma_{LV}}\kappa + \cos\,\theta_{CL}, \qquad (3)$$

which indicates the dependence of the contact angle θ_{LT} on κ, i.e., a dependence on the size of the droplet. Unlike the surface tension γ_{LV}, which must be positive, thermodynamic arguments do not give information about the sign of the line tension, i.e., τ_ℓ can be either positive or negative.[5,8] At present, the equilibrium molecular dynamics (EMD) method can be used to simulate a cap-shaped hemispherical nanoscale liquid droplet on a solid surface. This is a powerful alternative to solving the variational problem in order to obtain the apparent contact angle θ_{LT} and

κ for various sized droplets (see also Appendix B). Such geometrical analyses predicted a magnitude of τ_ℓ, which is around several pN ($\times 10^{-12}$ N),[9,10] indicating that the size effect is negligibly small for ordinary visible droplets. Nevertheless, recent experimental observations of nanometer-sized droplets and bubbles showed that these nanodroplets and nanobubbles have a pancake-like flat shape,[11,12] and it was also indicated from MD simulations that such a shape cannot be explained simply by Young's equation (1). A certain mechanism to pin the CL at such scales seems to be needed, and line tension may play a key role in the CL pinning.

Meanwhile, Kirkwood and Buff[13] developed a framework of surface tension from a viewpoint of statistical mechanics. This is a mechanical approach considering the molecular interactions based on a microscopic stress description.[14] In this molecular scale, an interface is explicitly dealt with as a region with a non-zero thickness where the physical properties change continuously, and the stress is not isotropic even in static equilibrium (see also Fig. 1). The integral of stress anisotropy around the liquid–vapor or liquid–gas interface can be related to the surface tension,[4,5,13,15] a process pioneered by Bakker.[16] Such a mechanical calculation of surface tension γ_{LV} through Bakker's equation using a quasi-one-dimensional (1D) flat liquid film system is considered a standard MD approach because it is easily realized by using the periodic boundary conditions (PBCs) in the surface–lateral directions.[17] Note that only the integral of each principal stress component in the whole system is used for the calculation of γ_{LV}, i.e., one does not need to obtain stress distributions, which is computationally demanding and not straightforward for systems with long-range Coulomb interactions.[18]

Regarding wetting, including solids, beyond simple evaluation of the apparent CA from the shape, a number of MD and Monte Carlo (MC) studies have been done mainly to quantitatively extract the SL and SV interfacial tensions through a thermodynamic and/or a mechanical approach.[9,19–44] Especially related to the latter, called the mechanical route, calculating the local stress distribution is one
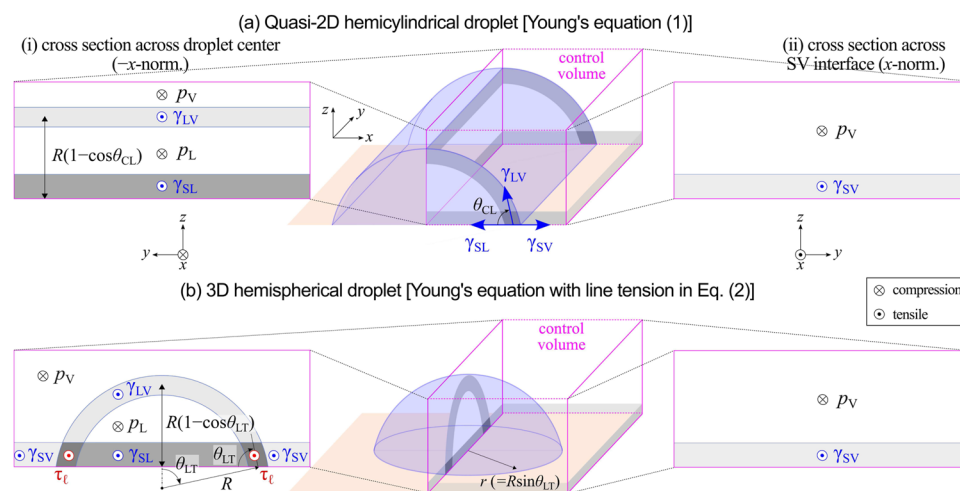
FIG. 1. A mechanical interpretation of Young's equation (1) and the line tension modification in Eq. (2), considering the equilibrium force balance on the rectangular control volumes (CVs) depicted in magenta.

of the key issues for the understanding of wetting through the connection to macroscopic fluid mechanics.[18] From the visualization of the stress field at the molecular scale using a quasi-two-dimensional (2D) system achieved under the PBC,[26,45,46] it has been shown that the stress anisotropy also exists at the SL and SV interfaces with finite thicknesses and that the CL is a local region where SL, LV, and SV interfaces with finite thicknesses meet and has more complex stress features (see Fig. 1 and also Fig. 8 in Appendix A). The present authors showed that γ_{SL} or γ_{SV} can be obtained by calculating the stress distribution along the direction normal to the solid surface away from the CL region and proved that the expression was consistent with Young's equation (1) by considering a control volume (CV) surrounding the CL and by determining the contact angle θ_{CL} from the extrapolation of the LV interface shape.[29] In other words, the force balance on the CV faces away from the CL is considered, and the CL region having a complex stress distribution is not explicitly included in Young's equation (1) in this quasi-2D framework.

Related to these studies, in this work, we provide one possible intuitive justification about the equilibrium force balance of Young's equation in Eq. (1) and modified one in Eq. (2) here. Figure 1 shows the CVs with one face passing through the center of the quasi-2D and three-dimensional (3D) equilibrium droplets of radius R and contact angle θ_{CL} or θ_{LT}, respectively. Both have a LV-interface with a uniform curvature. The anisotropic stress features mentioned above are schematized in these figures (see also Fig. 8), and the CL is considered to be a region where three interfaces, each with a finite thickness, meet. Now, we think about the equilibrium force balance on the control volumes (CVs) shown in magenta in the center of Fig. 1 with two parallel wall-normal faces: one set across the droplet center and the other set across the solid–vapor interface. This setting is, indeed, similar to the explanation of the Young–Laplace equation without solid by Berry.[47] The shear stress τ_{zx}, defined as the stress in the x-direction on a face with outward normal in the z-direction, is zero on the top face because it is in the vapor bulk. In addition, when the force from the solid is dealt with as an external force, i.e., not included in stress, the stress integral on the bottom face is zero because no fluid molecules exist below this bottom face.[29,48] Thus, under a condition with a flat and smooth solid wall where the external force from the solid, which can be assumed to be zero, the force balance on these CVs is expressed by the τ_{xx} components on the x-outward-normal and $-x$-outward-normal faces displayed in Figs. 1(i) and 1(ii). In the case of the quasi-2D droplet in Fig. 1(a), by ignoring the thicknesses of the interfaces, the force balance in Figs. 1(a-i) and 1(a-ii) is written by

$$\gamma_{LV} + \gamma_{SL} - p_L R(1 - \cos\theta_{CL}) = \gamma_{SV} - p_V R(1 - \cos\theta_{CL}), \quad (4)$$

where p_L and p_V denote the pressure values in liquid and vapor bulks, respectively. By inserting the Young–Laplace equation for a cylindrical interface,

$$p_L - p_V = \frac{\gamma_{LV}}{R}, \quad (5)$$

original Young's equation (1) is derived, which obviously does not include τ_ℓ, i.e., the anisotropic stress on the CL.

Meanwhile, in the case of the quasi-3D droplet in Fig. 1(b), the force balance in Figs. 1(b-i) and 1(b-ii) is written by

$$\gamma_{LV} \cdot 2R\theta_{LT} + \gamma_{SL} \cdot 2r + 2\tau_\ell - p_L(R^2\theta_{LT} - rR\cos\theta_{LT})$$
$$= \gamma_{SV} \cdot 2r - p_V(R^2\theta_{LT} - rR\cos\theta_{LT}), \quad (6)$$

where τ_ℓ is assumed to be positive if it gives a tensile force on the CL region. By inserting again the Young–Laplace equation for a spherical interface,

$$p_L - p_V = \frac{2\gamma_{LV}}{R}, \quad (7)$$

and the following geometrical relation

$$\frac{1}{\kappa} = r = R\sin\theta_{LT}, \quad (8)$$

Young's equation including line tension τ_ℓ in Eq. (2) is derived.

Indeed, Bey et al.[8] proposed a novel approach to extract τ_ℓ from similar quasi-2D EMD systems as an extension of the mechanical approach, without the need for the local stress distribution, and examined the dependence of τ_ℓ on the CA controlled by the solid–fluid interaction strength. They adopted a system with a quasi-2D droplet sandwiched between two parallel walls, i.e., a system with two menisci, and obtained τ_ℓ from the stress integral on the face normal to the CLs and geometric information obtained from the interface shape. Note that this stress integral corresponds to that on the y-normal face in Fig. 1(a), which includes the contribution from line tension.

For the thermodynamic approach, called the thermodynamic route, the SL and SV interfacial tensions were interpreted as the interfacial free energy per area obtained through the thermodynamic integration (TI) method.[28–36] Generally, the TI is a method to calculate the relative free energy of a target system as the difference from a reference system by connecting the target and reference systems with a thermodynamically reversible path using a coupling parameter embedded in the system Hamiltonian. As one possible implementation of the TI for the calculation of interfacial tension, Leroy et al. proposed the phantom-wall (PW) method[31,32] and the dry-surface (DS) method[33] described in detail in Sec. II. Briefly, as shown in Fig. 2(a), a quasi-1D EMD system with a flat SL interface was used as a target system of interest in these methods, and this target system was quasi-statically substituted by a reference system with bare solid (denoted by subscript "0") and liquid surfaces along a thermodynamic path with a constant number of particles N, temperature T and volume V or pressure p in a NVT- or NpT-ensemble. As a result, the minimum work needed for this change can be estimated as the Helmholtz or Gibbs free energy difference ΔF or ΔG, respectively, and is directly related to γ_{SL} as

$$w_{SL} \equiv \frac{\Delta F(\text{or } \Delta G)}{S} \approx \gamma_{S0} + \gamma_{LV} - \gamma_{SL} = -(\gamma_{SL} - \gamma_{S0}) + \gamma_{LV}, \quad (9)$$

where w_{SL} is called the SL Work of Adhesion (WoA) as the free energy per area S and $\gamma_{SL} - \gamma_{S0}$ is the interfacial free energy of the SL interface relative to that of the bare solid surface exposed to vacuum denoted by S0. In the PW method, a virtual wall called the "phantom-wall" interacting only with the fluid is used to strip the liquid off the solid surface by quasi-statically moving up. With this PW method, vacuum is inserted upon the lift-up as shown
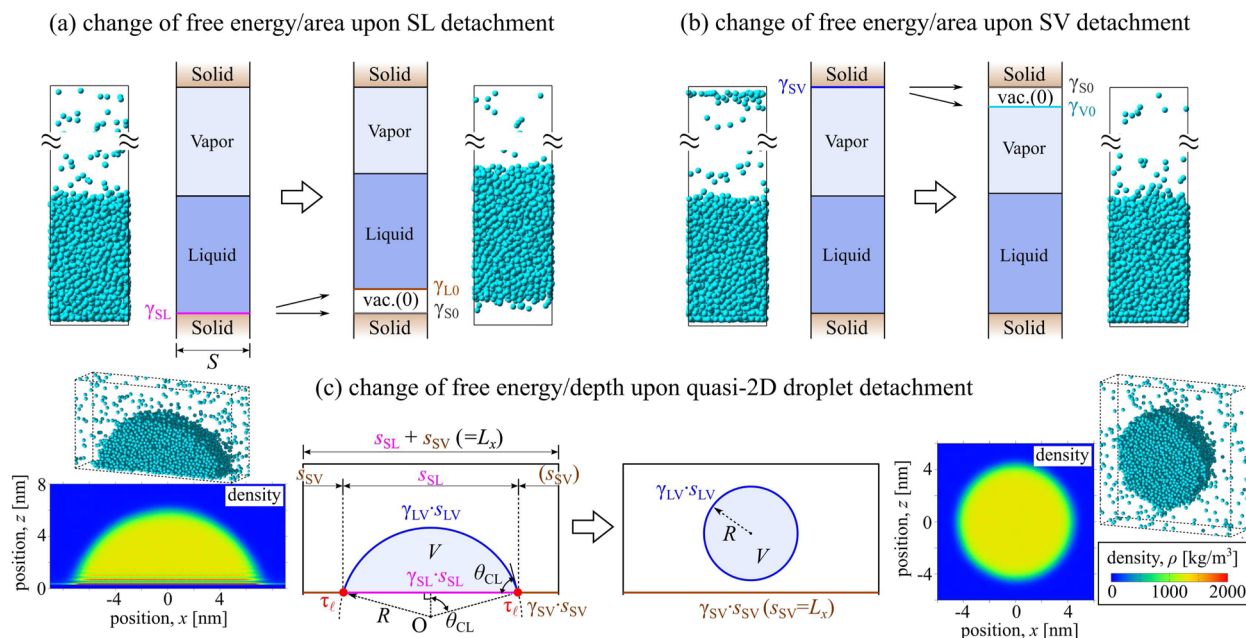
FIG. 2. Schematics of the thermodynamic integration (TI) method applied to quasi-1D systems to calculate the (a) solid–liquid (SL) and (b) solid–vapor (SV) interfacial tensions γ_{SL} and γ_{SV}, respectively, from the change of free energy per area obtained upon the quasi-static detachment of the SL and SV interfaces. (c) Schematic of the DS method extended to the quasi-2D droplet systems to calculate the line tension τ_ℓ.

in Fig. 2(a), and a NpT-ensemble is used, e.g., by controlling the pressure using the solid as the piston.

This method is advantageous because it is applicable to various kinds of SL combinations with various solid–liquid interaction potential forms.[36,49] Meanwhile, in the DS method, the coupling parameter is assigned to a specific SL interaction parameter. With this DS method, a reference system equivalent to that in Fig. 2(a) with the solid and liquid detached is reproduced by setting the SL interaction to be mostly repulsive. In this case, vacuum is not inserted and both NVT and NpT ensembles can be used because the effect of the resulting change of the vapor volume is negligibly small. The DS method is powerful in the sense that the SL interfacial tension can be obtained as a semi-continuous function of the SL interaction parameter.[29,35] Similarly, the SV interfacial tension γ_{SV} can also be evaluated from the SV work of adhesion w_{SV} using a system shown in Fig. 2(b), which is also described in detail in Sec. II.

Regarding the TI calculation of the interfacial free energy, the cleaving methods were proposed to analyze the crystal–melt interfaces,[50–52] where a more complex thermodynamic path was considered to guarantee the reversibility because the fragile interface structure composed of identical solid and liquid components was sensitive to the path, i.e., interface structure was easily deformed upon the crystal–melt separation procedure. Meanwhile, simpler TI schemes mentioned above are preferred due to their implementational simplicity for the analysis of wetting especially between a liquid and a rigid or hard solid where the Shuttleworth effect is negligible.[53,54]

Based on these mechanical and thermodynamic routes, we obtained γ_{SL} or γ_{SV} using a quasi-1D system with a flat SL or SV interface with various solid–fluid combinations and showed that the CA predicted from these values corresponded well with the apparent CA of a quasi-2D droplet formed on the solid wall with the same solid–fluid interaction parameters.[11,26,28,29,36] These studies indicated that the apparent CA of the droplet obtained in the MD simulations agreed well with the one predicted by Young's equation (1) in case the solid surfaces are flat and smooth so that the CL pinning cannot be induced.

An important and interesting point about these results is that the CA of a quasi-2D droplet, without including line tension τ_ℓ, can be estimated from the interfacial tensions γ_{SL}, γ_{SV}, and γ_{LV} obtained by mechanical and thermodynamic approaches in quasi-1D systems without CL. Meanwhile, Bey et al.[8] extracted line tension τ_ℓ from quasi-2D systems with straight CLs of zero curvature by a mechanical approach considering the stress integral on the face normal to the CL.

In this study, as a thermodynamics approach, we propose an extension of the DS method to extract τ_ℓ by evaluating the free energy difference from a reference system as illustrated in Fig. 2(c) through the quasi-static detachment of a quasi-2D hemicylindrical droplet. The key concept is that we calculate the free energy difference $\Delta F_{drop}/L$ per unit depth (L: system depth) given by

$$\frac{\Delta F_{drop}}{L} = \Delta[\gamma_{LV} \cdot s_{LV}] + \Delta[\gamma_{SL} \cdot s_{SL}] + \Delta[\gamma_{SV} \cdot s_{SV}] + 2\tau_\ell, \quad (10)$$

where the free energy is given as the sum of the energy of two lines $2\tau_\ell$ and the interfacial energies of LV, SL, and SV interfaces with lengths s_{LV}, s_{SL}, and s_{SV}, respectively. Note again that τ_ℓ has units of

energy/length. In addition, the dependence of τ_ℓ on the solid–fluid interaction strength was examined and was also compared with the result by Bey *et al.*[8] and that estimated from the size dependence of the CA of 3D droplets based on Eq. (3) shown in Appendix B.

II. METHOD

A. MD simulation systems

In this study, we employed two types of equilibrium MD simulation systems: (a) quasi-one-dimensional (1D) systems with flat solid–liquid (SL) and solid–vapor (SV) interfaces and (b) quasi-two-dimensional (2D) droplet systems with a hemi-cylindrical droplet on a solid surface as shown in Fig. 3. As the constituent fluid molecules, generic particles with the inter-particle interaction described by the 12-6 Lennard-Jones (LJ) potential were used. The 12-6 LJ potential expressed by

$$\Phi_{ff}(r_{ij}) \equiv \Phi^{LJ}(r_{ij}) = 4\varepsilon_{ff}\left[\left(\frac{\sigma_{ff}}{r_{ij}}\right)^{12} - \left(\frac{\sigma_{ff}}{r_{ij}}\right)^6 + c_2^{LJ}\left(\frac{r_{ij}}{r_c}\right)^2 + c_0^{LJ}\right] \quad (11)$$

was adopted for the interaction between fluid particles as a function of the distance r_{ij} between the particle i at position r_i and

j at r_j, with ε and σ being the LJ energy and length parameters, respectively. A cutoff distance of $r_c = 3.5\sigma_{ff}$ was used for this LJ interaction, and by adding quadratic functions, the potential and interaction force smoothly approached zero at r_c. The values of the constants c_2^{LJ} and c_0^{LJ} as functions of r_c and σ_{ff} are shown in our previous study.[26] The fluid particles are expressed by "f" and the corresponding interactions are denoted by subscripts hereafter.

Both systems in Figs. 3(a) and 3(b) have two solid walls on the bottom and top of the simulation cell shown in light-red. To minimize the number of arbitrary parameters affecting the basic physics of wetting, the solid wall was modeled by a simple one-dimensional potential field interacting with the fluid particles as a function of the distance rather than modeling a group of solid particles. The interaction Φ_{sf} between the immobile top or bottom solid wall at $z = z_s^{top}$ or $z = z_s^{bot}$, respectively, and the fluid particle at $z = z_i$ was given by

$$\Phi_{sf}(z_i'; \eta) = 4\pi\rho_n\varepsilon_{sf}\sigma_{sf}^2\left[\frac{1}{5}\left(\frac{\sigma_{sf}}{z_i'}\right)^{10} - \frac{1}{2}\left(\frac{\sigma_{sf}}{z_i'}\right)^4 + c_2^{sf}\left(\frac{z_i'}{z_c}\right)^2\right.$$
$$\left. + c_1^{sf}\left(\frac{z_i'}{z_c}\right) + c_0^{sf}\right], \quad (12)$$
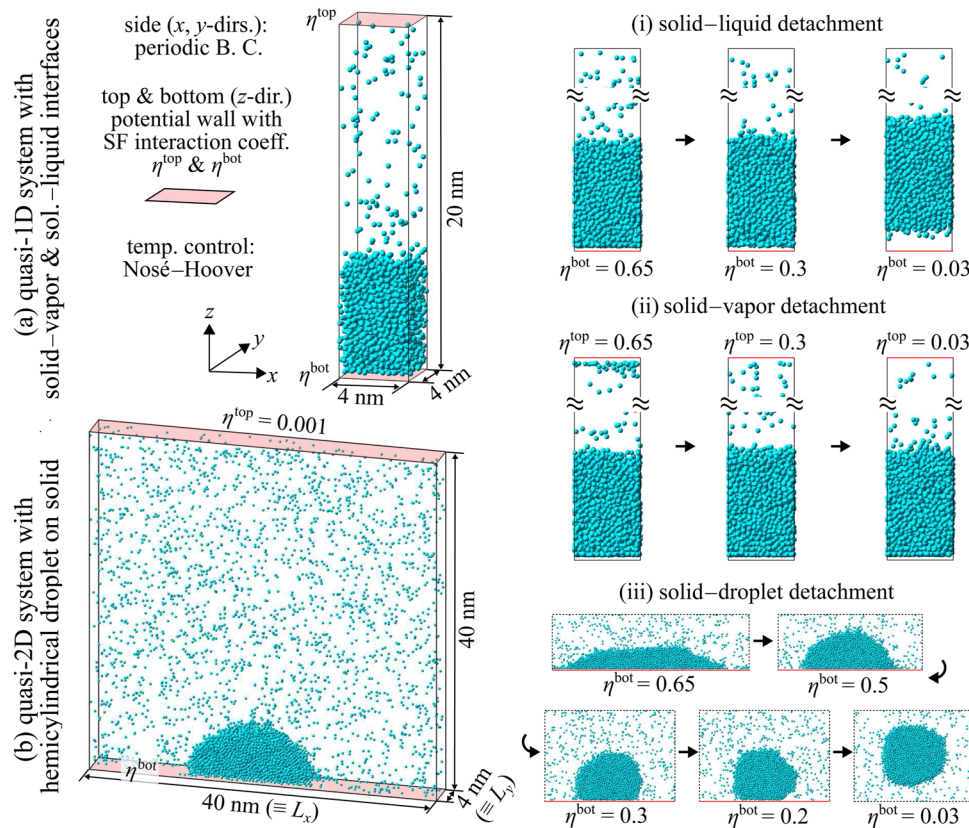
FIG. 3. (a) Quasi-one-dimensional (1D) system with liquid and vapor attached on the bottom and top solid surfaces, respectively, and schematics of the (i) solid–liquid detachment and (ii) solid–vapor detachment processes performed by changing the solid–fluid interaction parameter η^{bot} or η^{top} of the bottom or top surface, respectively. (b) Quasi-two-dimensional (2D) system with a hemi-cylindrical liquid droplet on the solid surface on the bottom, and (iii) schematic of the solid–droplet detachment process in the quasi-2D system.

with

$$\varepsilon_{sf} = \eta \varepsilon_{sf}^0, \quad z_i' = z_s^{top} - z_i, \quad \text{or} \quad z_i' = z_i - z_s^{bot}. \quad (13)$$

This potential field corresponds to a mean potential field created by a single layer of uniformly distributed solid particles with an area number density ρ_n, which interact with the fluid particles through the LJ potential with the energy and length parameters being $\varepsilon_{sf}(= \eta \varepsilon_{sf}^0)$ and σ_{sf}, respectively, where the solid–fluid (SF) interaction parameter η was multiplied to the base value of ε_{sf}^0 of 1.29×10^{-21} J as described below. Similar to Eq. (11), this potential field in Eq. (12) was truncated at a cutoff distance of $z_c = 3.5\sigma_{sf}$ with a quadratic function so the potential and interaction force smoothly vanished at z_c.

The quasi-1D system in Fig. 3(a) contained 2000 fluid particles in a simulation cell of $4 \times 4 \times 20$ nm³ with the top and bottom walls modeled by Eq. (12) with $z_s^{top} = 20$ nm and $z_s^{bot} = 0$, respectively. Meanwhile, the quasi-2D system in Fig. 3(b) contained 7000 fluid particles in a simulation cell of $40 \times 4 \times 40$ nm³ with the top and bottom walls at $z_s^{top} = 40$ nm and $z_s^{bot} = 0$. The periodic boundary condition was applied in the wall lateral x- and y-directions for both systems. With this system size, as shown later in the density distributions in Fig. 5, sufficiently large bulk liquid volume excluding the interface thicknesses was formed for the each droplet in Fig. 3(b) (see also Fig. 1), and this was also achieved for the thickness of the bulk liquid in Fig. 3(a).[29] In addition, the droplet radius was sufficiently larger than the size range where the curvature dependence of the surface tension γ_{LV} should be considered, known as the Tolman correction.[15,55] Hence, with this condition, the results were not sensitive to the system size.

The system temperature was maintained at a constant temperature T by using the Nosé–Hoover thermostat with an effective mass Q of $3N_f k_B T \tau^2$ with $\tau = 1.0 \times 10^{-12}$ s applied to all fluid particles, where N_f is the number of fluid particles. Note that the choice of Q had a negligible effect on the results for the present equilibrium systems after a sufficient relaxation run. For the temperature, we have chosen $T = 100$ K, which is between the triple point and critical temperatures.[56] Note that the temperature control had no effects on the results since in this study we deal with fully relaxed equilibrium systems, including the detachment processes in Figs. 3(i)–3(iii) explained below. The velocity Verlet method was applied for the integration of the Newtonian equation of motion with a time step of 5 fs for all systems. The simulation parameters are summarized in Table I with the corresponding non-dimensional ones, which are normalized by the corresponding standard values based on ε_{ff}, σ_{ff}, and mass m_f.

The SF interaction parameter η for the top and bottom walls was set at η^{top} and η^{bot}, respectively, and they were changed in a parametric manner except for the top wall in Fig. 3(b) fixed at $\eta^{top} = 0.001$. With the present setup, a hemi-cylindrical droplet was formed on the bottom wall as an equilibrium state in the quasi-2D system in Fig. 3(b), and as indicated in Fig. 3(iii), the contact angle θ_{CL} of the droplet had a one-to-one correspondence with the value of η for the bottom wall at a given temperature, i.e., η expresses the wettability. This is the case for the present solid modeled by a potential field exerting no wall-tangential force on the fluid as an ideally smooth solid surface without inducing pinning of the CL.[26,29,30] Note that in the present quasi-2D systems, the effects of the CL curvature

TABLE I. Simulation parameters and their corresponding non-dimensional values.

Property	Value	Unit	Non-dim. value
σ_{ff}	0.340	nm	1
ε_{ff}	1.67×10^{-21}	J	1
σ_{sf}	0.345	nm	1.015
ε_{sf}^0	1.29×10^{-21}	J	1.18
ρ_n	3.61^2	nm⁻²	1.23^2
ε_{sf}	$\eta \times \varepsilon_{sf}^0$		
η	0.03–0.65	⋯	⋯
m_f	6.64×10^{-26}	kg	1
T	100	K	0.827
N_f (quasi-1D)	2000	⋯	⋯
N_f (quasi-2D)	7000	⋯	⋯

can be neglected.[7,9,24,26,29,30,32,57] Meanwhile, with a narrow lateral size, a quasi-1D liquid film attached on the bottom wall was formed as an equilibrium state as in Fig. 3(a) by setting $\eta^{bot} > \eta^{top}$ with η^{bot} giving a droplet contact angle θ_{CL} below 180°.

The physical properties of each equilibrium system with various η values were calculated as the time average of 30 and 50 ns for the quasi-1D and quasi-2D systems, respectively, both started from an equilibration run of more than 10 ns.

B. Dry-surface method

The thermodynamic integration (TI) is a method to determine the free energy difference of two equilibrium states by connecting them with a quasi-static path through a TI parameter embedded in the system Hamiltonian. Let λ be the TI parameter, and let the target and reference systems correspond to $\lambda = 0$ and $\lambda = 1$ described by the system Hamiltonian $H(\Gamma, \lambda)$ in a constant NVT system as a function of all positions and momenta Γ, i.e., the phase space variable. Then, the difference of the Helmholtz free energy between the two systems is written as

$$\Delta F \equiv \left[F(N, V, T; \lambda) \right]_{\lambda=0}^{\lambda=1} = \int_0^1 \left(\frac{\partial F}{\partial \lambda} \right)_{N,V,T} d\lambda. \quad (14)$$

By using the relation between the Helmholtz free energy F and the configurational partition function Z, it follows for Eq. (14) that

$$\Delta F = -k_B T \int_0^1 \frac{1}{Z} \left(\frac{\partial Z}{\partial \lambda} \right)_{N,V,T} d\lambda = \int_0^1 \left\langle \frac{\partial H}{\partial \lambda} \right\rangle_\lambda d\lambda, \quad (15)$$

where the angular brackets denote the ensemble average. Note that this ensemble average depends on λ as indicated by the subscript of the angular brackets. If the system Hamiltonian H is analytically differentiable with respect to λ, i.e., $\frac{\partial H}{\partial \lambda}$ can be calculated for each microscopic system, the integrand in the right-most hand side of Eq. (15) is the ensemble average with a given λ. Note that in practice, multiple equilibrium MD systems of λ between 0 and 1 are prepared, and $\left\langle \frac{\partial H}{\partial \lambda} \right\rangle_\lambda$ is calculated in each system as the time average instead of ensemble average assuming ergodicity. A similar relation can be derived for the Gibbs free energy difference in constant NpT systems.[29,31,32]

Leroy and Müller–Plathe[33] proposed the DS to calculate the SL interfacial tension through a fluid stripping process from the solid surface by embedding the TI parameter λ into the SF interaction potential. Specifically in the present study, we include the TI parameter λ into the SF interaction in Eq. (12) expressed by the LJ potential as

$$\Phi_{\mathrm{sf}}^{\mathrm{DS}}(z_i'; \eta, \lambda) \equiv (1 - \lambda)\Phi_{\mathrm{sf}}(z_i'; \eta). \tag{16}$$

Then, for a constant NVT system, Eq. (14) is written by

$$\Delta F(\eta) = \int_0^{1^-} \left\langle \frac{\partial H}{\partial \lambda} \right\rangle_\lambda \mathrm{d}\lambda = -\int_0^{1^-} \left\langle \sum_{i=1}^{N_f} \Phi_{\mathrm{sf}}(z_i'; \eta) \right\rangle_\lambda \mathrm{d}\lambda. \tag{17}$$

Note that both the ensemble averages depend implicitly on λ. As λ approaches 1, the SF interaction is weakened, and the solid surface becomes "dry" for λ slightly smaller than 1 denoted by 1^-, because at $\lambda = 1$, the SF repulsion becomes zero and the fluid particles can freely pass through the solid wall. By considering the relation

$$\Phi_{\mathrm{sf}}(z_i'; \eta) = \eta \Phi_{\mathrm{sf}}(z_i'; \eta = 1) \tag{18}$$

in Eq. (12), and by changing the integration variable in the rightmost hand side of Eq. (17) from λ to ξ as

$$\xi = (1 - \lambda)\eta, \tag{19}$$

it follows

$$\Delta F(\eta) = -\int_{0^+}^\eta \left\langle \sum_{i=1}^N \Phi_{\mathrm{sf}}(z_i'; \eta = 1) \right\rangle_\xi \mathrm{d}\xi = -\int_{0^+}^\eta \frac{E_{\mathrm{sf}}(\xi)}{\xi} \mathrm{d}\xi, \tag{20}$$

with defining the ensemble average of the total SF interaction potential energy $E_{\mathrm{sf}}(\xi)$ at $\eta = \xi$ by

$$E_{\mathrm{SF}}(\xi) = \left\langle \sum_{i=1}^N \Phi_{\mathrm{sf}}(z_i'; \xi) \right\rangle_\xi, \tag{21}$$

where 0^+ denotes a value of ξ slightly larger than zero. For instance, it can be set at $\xi = 0.03$ with which the droplet is completely detached from the solid surface as displayed in Fig. 3(iii). Equation (20) means that we get the system trajectory with the corresponding SF interaction parameter $\eta = \xi$, whereas we calculate the ensemble average (substituted by the time average) of the total SF interaction potential energy $E_{\mathrm{SF}}(\xi)$ and divide it by ξ as the integrand to numerically integrate the right-most hand side. A remarkable advantage of the DS method is that Eq. (20) is in an integral form with η as the upper limit, i.e., the free energy difference $\Delta F(\eta)$ from the reference system can be obtained as a semi-continuous function of $\eta \in [0^+, \eta_{\max}]$, where $\eta_{\max}$ is the maximum value of η to be investigated. More concretely, we calculate multiple equilibrium systems with discrete ξ values between 0^+ and $\eta_{\max}$ with a sufficiently small increment $\mathrm{d}\xi$ and calculate the integrand $\frac{E_{\mathrm{SF}}(\xi)}{\xi}$ in Eq. (20) as the time average in each system; then, $\Delta F(\eta)$ is obtained as the integral from 0^+ up to $\eta \ (\leq \eta_{\max})$ by numerical integration.

III. RESULTS AND DISCUSSION

A. Works of solid–liquid and solid–vapor adhesion

Figure 2 shows the schematic of the DS method applied to quasi-1D systems to calculate the SL and SV interfacial tensions γ_{SL} and γ_{SV}, respectively, as the free energy per area obtained upon the quasi-static detachment of the SL and SV interfaces. To calculate the SL interfacial tension, we carried out the DS process of SL detachment as shown in Fig. 2(a), where η^{top} was kept constant at 0.001, whereas η^{bot} was changed from 0.1 to 0.7 ($=\eta_{\max}^{\mathrm{bot}}$). Upon this process, the original SL interface is separated into "dry" solid–vacuum and liquid–vacuum interfaces. We denote this vacuum by "0" hereafter. Then, the work of SL adhesion w_{SL} defined as the free energy per surface area S needed for this change is written as

$$w_{\mathrm{SL}}(\eta) \equiv \frac{\Delta F(\eta)}{S} = \gamma_{\mathrm{S0}} + \gamma_{\mathrm{L0}} - \gamma_{\mathrm{SL}}(\eta)$$
$$\approx \gamma_{\mathrm{S0}} + \gamma_{\mathrm{LV}} - \gamma_{\mathrm{SL}}(\eta), \tag{22}$$

where the subscript S0 denotes the bare solid surface without liquid or vapor adsorbed on it. Considering that the effect of the vapor density on the LV surface tension for the temperature range in this study is negligible, γ_{L0} was approximated by γ_{LV}. The value of γ_{LV} was obtained from a MD system with planar LV interfaces by a standard mechanical process in which the difference between the normal stress components vertical and parallel to the interface was integrated around the LV interface, which resulted in $\gamma_{\mathrm{LV}} = 7.47 \times 10^{-3}$ N/m at $T = 100$ K.[11,28]

Similarly, the DS process of SV detachment as shown in Fig. 2(b) was carried out to calculate the SV interfacial tension, where η^{bot} was kept constant at 1.0, whereas η^{top} was changed from 0.1 to 0.7 ($= \eta_{\max}^{\mathrm{top}}$). This detachment process separates the original SV interface into S0 and V0 interfaces, and the work of SV adhesion w_{SV} is expressed by

$$w_{\mathrm{SV}}(\eta) \equiv \frac{\Delta F(\eta)}{S} = \gamma_{\mathrm{S0}} + \gamma_{\mathrm{V0}} - \gamma_{\mathrm{SV}}(\eta)$$
$$\approx \gamma_{\mathrm{S0}} - \gamma_{\mathrm{SV}}(\eta) \tag{23}$$

assuming $\gamma_{\mathrm{V0}} \approx 0$. Note that w_{SL} and w_{SV} have the same dimension as the interfacial tensions. As described later, $\gamma_{\mathrm{SL}} - \gamma_{\mathrm{SV}}$ appearing in Young's equation can be calculated from Eqs. (22) and (23) by eliminating γ_{S0}.

Figure 4(a) shows the relation between the work of adhesion and the solid–fluid interaction coefficient η for the SL adhesion w_{SL} and the SV adhesion w_{SV} obtained through the DS method. With the increase in η, both works of adhesion w_{SL} and w_{SV} became large, and the work of SV adhesion had a non-negligible value for η above about 0.4, where an adsorption layer was formed at the SV interface as observed in Fig. 2(b). Along this quasi-static thermodynamic path, w_{SL} and w_{SV} were obtained as smooth functions of η through the DS scheme based on Eq. (20). We used these values to evaluate the contact angle θ_{CL} using the Young–Dupré equation, shown later in Eq. (32), as displayed in Fig. 4(b).
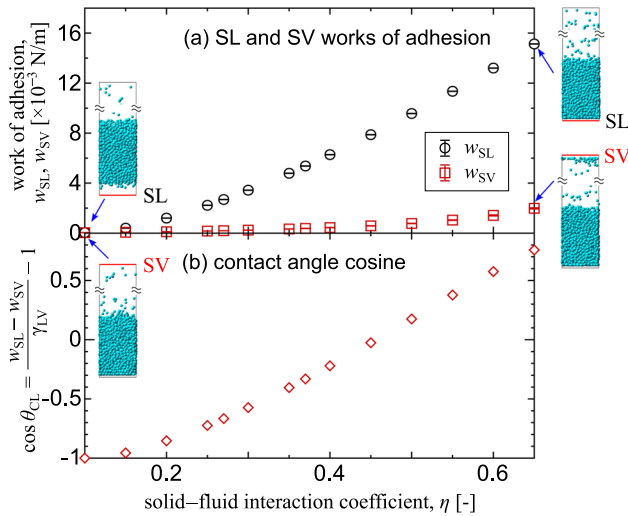
FIG. 4. (a) Relation between the work of adhesion and solid–fluid interaction coefficient η for SL and SV interfaces obtained through the DS method and (b) contact angle cosine estimated by the Young–Dupré equation (32).

FIG. 5. Work of droplet adhesion. Corresponding time-averaged density distributions around the center of mass of the quasi-2D droplets are shown on the top. The error bars are smaller than the size of symbol similar to those in Fig. 4(a).

B. Work of droplet adhesion

We extended the DS method to the quasi-2D droplet systems in Fig. 2(c) to calculate the line tension τ_ℓ. Similar to the quasi-1D DS process, the droplet detachment process was carried out for the quasi-2D system as illustrated in Fig. 2(c), where the free energy difference $\Delta F(\eta)$ as the numerical integral in Eq. (20) was calculated using multiple equilibrium systems with the SF interaction η between 0^+ and $\eta_{\max}$. Note that at $\eta = 0^+ \ll 1$, the droplet was detached from the bottom wall. Figure 5 shows the work of droplet adhesion W_{drop} defined as the free energy per system depth L_y needed to strip off the hemi-cylindrical quasi-2D droplet from the solid surface. Note that W_{drop} has the same dimension as force. The corresponding time-averaged density distributions around the center of mass of the droplet for several η values are also displayed on the top panel. The qualitative feature of W_{drop} was the same as w_{SL} in Fig. 4, i.e., it increased with the increase in η, and was obtained as a semi-smooth function of η owing to the advantage of the DS method. It was also indicated from the time-averaged density distributions on the top panel that the LV interface away from the solid had a spherical interface with a uniform curvature surface.

Note that one underlying hypothesis of a TI model between two configurations of the system is that the thermodynamic path between these two is reversible, i.e., the end points of the thermodynamic path are unique equilibrium states. In other words, in the present case, the same value $\frac{E_{\mathrm{sf}}(\eta)}{\eta}$ as the average of the total SF interaction energy (over η) must be obtained as the integrand in Eq. (20) independent of the path to obtain a unique W_{drop} value, e.g., through the forward path from left to right in Fig. 5, or through the inverted path right to left without hysteresis. Indeed, we prepared the systems of various η values starting from independent initial configurations with a rather arbitrary manner. As indicated in the snapshot in Fig. 3(iii) and in the density distribution in Fig. 5, the resulting droplet was basically detached from the bottom wall for
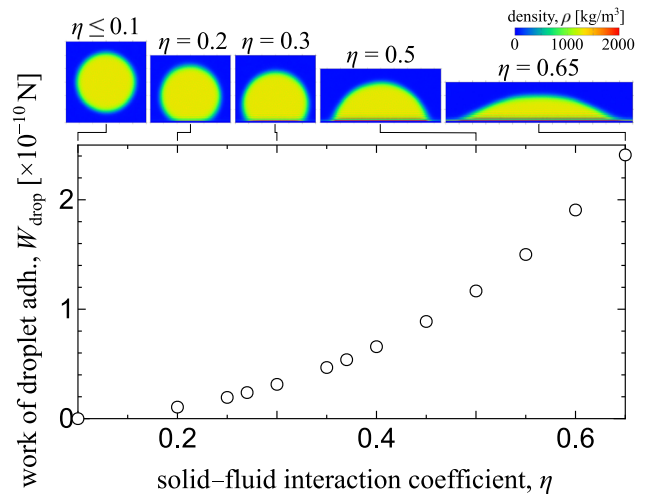
$\eta \leq 0.1$. In such a system, the droplet bounced off the bottom and top walls and was occasionally attached on the bottom wall, i.e., a unique equilibrium state was not obtained. However, the average absolute value of $\frac{E_{\mathrm{sf}}(\eta)}{\eta}$ was small for $\eta \leq 0.1$ within the error bars, which were smaller than the symbols in Fig. 5 irrespective of whether the droplet was flying in the vapor or attached on the bottom wall because the SF interaction was very weak, and the hysteresis effect on the present result was supposed to be negligibly small. This is also seen in the smooth increase in W_{drop} with the increase in η in Fig. 5. Related to this point, the setting of the lower end of 0^+ in Eq. (20) at $\xi = 0.03 \ (\equiv 0^+)$ gave a small error for the present case.

We assume that the change in bulk liquid and vapor volumes upon the change in η is negligibly small, i.e., the total free energy of the bulk regions is kept constant and the change in the system free energy is due to the interface and CL upon the droplet detachment process. Then, W_{drop} is written as

$$
\begin{aligned}
W_{\mathrm{drop}}(\eta) &\equiv \frac{\Delta F_{\mathrm{drop}}(\eta)}{L_y} \\
&= \Delta[\gamma_{\mathrm{LV}} \cdot s_{\mathrm{LV}}(\eta)] + \Delta[\gamma_{\mathrm{SL}}(\eta) \cdot s_{\mathrm{SL}}(\eta)] \\
&\quad + \Delta[\gamma_{\mathrm{SV}}(\eta) \cdot s_{\mathrm{SV}}(\eta)] + 2\Delta\tau_\ell(\eta),
\end{aligned} \tag{24}
$$

where s_{LV}, s_{SL}, and s_{SV} denote the lengths of the corresponding interface projected in the xz-plane, and the values with (η) mean that they depend on the SF interaction parameter η. By assuming that γ_{LV} is independent of η, i.e., independent of the curvature of the LV interface for the present droplet size range,[55] and by inserting Eqs. (22) and (23) into Eq. (24), it follows

$$
\begin{aligned}
W_{\mathrm{drop}}(\eta) &= \gamma_{\mathrm{LV}} \cdot \Delta s_{\mathrm{LV}}(\eta) + w_{\mathrm{SV}}(\eta) \cdot L_x \\
&\quad - (w_{\mathrm{SV}}(\eta) - w_{\mathrm{SL}}(\eta) + \gamma_{\mathrm{LV}}) s_{\mathrm{SL}}(\eta) - 2\tau_\ell(\eta), \tag{25}
\end{aligned}
$$

where the simple length relation $s_{\mathrm{SL}} + s_{\mathrm{SV}} = L_x$ with L_x being the system size in the x-direction is used, and we set $\tau_\ell(\eta) = 0$ for $\eta \approx 0$

with the droplet detached from the solid surface. Hence, if the two lengths Δs_{LV} and s_{SL} are determined as a function of η, then τ_ℓ can be obtained using $w_{SL}(\eta)$, $w_{SV}(\eta)$, and $W_{drop}(\eta)$ as

$$\tau_\ell(\eta) = \frac{1}{2}\big[\gamma_{LV} \cdot \Delta s_{LV}(\eta) + w_{SV}(\eta) \cdot L_x$$
$$+ (w_{SL}(\eta) - w_{SV}(\eta) - \gamma_{LV})s_{SL}(\eta) - W_{drop}(\eta)\big]. \quad (26)$$

However, considering that τ_ℓ is small,[8] the results may depend strongly on the definition of the geometric parameters $\Delta s_{LV}(\eta)$ and $s_{SL}(\eta)$ in Eq. (26). To reduce the statistical error due to the fluctuation, we define these geometric parameters by determining the value of the droplet volume V, i.e., the droplet area $A \equiv V/L_y$ projected onto the xz-plane, which we assumed to be constant independent of η in Eq. (24) so that they are consistent with the works of adhesion $w_{SL}(\eta)$ and $w_{SV}(\eta)$ and are semi-smooth functions of η as in Figs. 4 and 5. As a geometrical relation [see Fig. 2(c)], the droplet area A is given by

$$A \equiv \frac{V}{L_y} = R^2(\theta_{CL} - \cos\theta_{CL}\sin\theta_{CL}) \quad (27)$$

using the contact angle θ_{CL} as a function of η and the radius of the 2D-droplet R. By determining A_c and its error δA_c from the average of the projected droplet area A for various η values (see the supplementary material), the radius $R(\theta_{CL}(\eta))$ is determined by

$$R(\theta_{CL}(\eta)) = \sqrt{\frac{A_c}{\theta_{CL}(\eta) - \cos\theta_{CL}(\eta)\sin\theta_{CL}(\eta)}} \quad (28)$$

as a function of the contact angle $\theta_{CL}(\eta)$, and its uncertainty is also estimated using Eq. (28). By using $\theta_{CL}(\eta)$ and $R(\theta_{CL}(\eta))$ given by Eq. (28), the geometric parameters $s_{SL}(\theta_{CL}(\eta))$ and $\Delta s_{LV}(\theta_{CL}(\eta))$ are expressed as a function of $\theta_{CL}(\eta)$ as well by

$$s_{SL}(\theta_{CL}(\eta)) = 2R(\theta_{CL}(\eta))\sin\theta_{CL}(\eta) \quad (29)$$

and

$$s_{LV}(\theta_{CL}(\eta)) = 2R(\theta_{CL}(\eta))\theta_{CL}(\eta), \quad (30)$$

$$\Delta s_{LV}(\theta_{CL}(\eta)) \equiv s_{LV}(\pi) - s_{LV}(\theta_{CL}(\eta)), \quad (31)$$

respectively, where $s_{LV}(\pi) = 2\sqrt{\pi A_c}$ is the circumference of a circle with an area A_c. Thus, if the contact angle $\theta_{CL}(\eta)$ is obtained as a semi-smooth function of η, the geometric parameters in Eqs. (29) and (31) can be written as semi-smooth functions of η as well, and, consequently, τ_ℓ in Eq. (26) is determined.

Now, the agenda is how to obtain $\theta_{CL}(\eta)$ as a function of η to be consistent with the works of adhesion and how to determine the constant volume (area in the xz-plane) A_c in Eq. (28). For the former, it has been shown in our previous study that the following Young–Dupré equation holds for a droplet on a flat and smooth solid surface:

$$\cos\theta_{CL} = \frac{-\gamma_{SL} + \gamma_{SV}}{\gamma_{LV}} = \frac{-(\gamma_{SL} - \gamma_{S0}) + (\gamma_{SV} - \gamma_{S0})}{\gamma_{LV}}$$
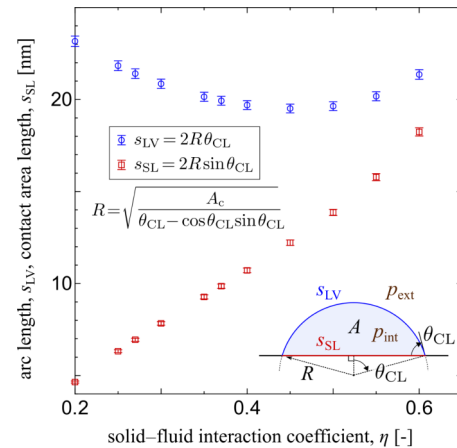$$= \frac{w_{SL}(\eta) - w_{SV}(\eta)}{\gamma_{LV}} - 1, \quad (32)$$

FIG. 6. Geometric parameters s_{LV} and s_{SL} obtained each as a function of η.

which is rewritten by using Eqs. (22) and (23). The relation between θ_{CL} and η obtained from Eq. (32) using $w_{SV}(\eta)$ and $w_{SL}(\eta)$ in Fig. 4(a) is shown in Fig. 4(b). The CA, indeed, agreed well with the apparent CA, e.g., estimated from the density distributions in the top panel of Fig. 5, since the solid surface in the present study is ideally smooth.[29]

Meanwhile, for the projected area A_c, a difficulty exists in the definition of the radius R to determine the volume because the interface is not a surface of discontinuity but a region with a certain thickness at the nanoscale. A possible and common choice is using the Gibbs dividing surface,[58] and another choice as a strict mechanical definition based on the force and momentum balance was also suggested.[55] Considering that we assume γ_{LV} to be constant and also that the LV interface has a uniform curvature, we used the Young–Laplace equation (quasi-2D) to determine the radius R for each system with various η (see the supplementary material). The pressure difference Δp was estimated from the stress distribution in the droplet or surface normal pressure distributions on the solid wall from the fluid in the present study. The calculation methods and examples of the stress distribution and the wall normal force distribution to obtain Δp are shown in Appendix A.

Figure 6 shows the geometric parameters s_{LV} and s_{SL} expressed as a function of η. As easily imagined, the contact area s_{SL} increased with the increase in η, whereas the LV interface area s_{LV} showed different dependences on η. For both s_{SL} and s_{LV}, the error bars mainly due to the estimation of the area A_c were not remarkably large.

Now, all the values $R(\theta_{CL})$, $s_{SL}(\theta_{CL})$, and $\Delta s_{LV}(\theta_{CL})$ in Eqs. (28), (29), and (31) each as a function of the contact angle θ_{CL} can be determined for a given θ_{CL} value, which is directly related to the solid–fluid interaction coefficient η by Eq. (32), meaning that τ_ℓ in Eq. (26) can be determined as a function of θ_{CL} or η. Figure 7 shows line tension τ_ℓ as a function of the contact angle θ_{CL} obtained by the present thermodynamic approach, superimposed on the result obtained by Bey *et al.*[8] from a mechanical approach, and that evaluated by Eq. (3) from the size dependence of the CA as a simple geometrical approach (see Appendix B). The corresponding η value is displayed on the top horizontal axis obtained by the relation between η and θ_{CL} in Fig. 4(b). In Ref. 8, as briefly described
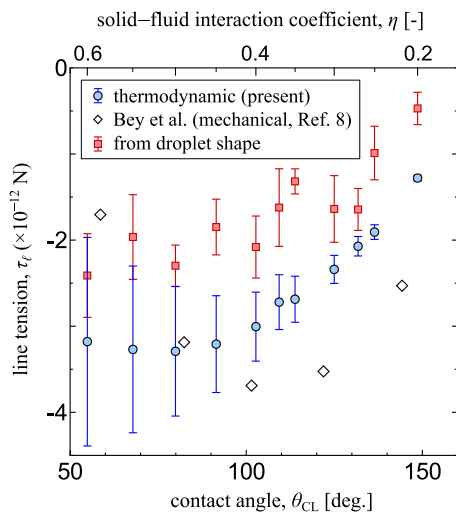
FIG. 7. Line tension τ_ℓ vs contact angle θ_{CL} in comparison with the result by Bey *et al.*[8] from a mechanical approach using systems with a LJ droplet sandwiched between structure-less potential walls, which were similar to the present study, and that evaluated by Eq. (3) from the size dependence of the droplet CA (see Appendix B). All systems were at the same temperature. The corresponding η value on the top horizontal axis is evaluated by the θ_{CL}–η relation in Fig. 6(a). Only the data of the largest liquid bridges from Bey *et al.*[8] is shown.

in Sec. I, they used equilibrium MD systems with a LJ droplet sandwiched between structure-less potential walls, which were similar to the present study, while a different cutoff length of $4\sigma_{ff}$ for the LJ interaction and a different wall potential form instead of Eq. (12) were used. They varied the wettability parameter (η in our case) and obtained τ_ℓ from the stress integral, i.e., three average values of the principal stress, and geometric information including the contact area and CA obtained from the interface shape. They also changed the temperature as well as the droplet size with changing the inter-wall distance h to examine the confinement effect, however; in the present figure, we showed their data only of the largest liquid bridges ($h \approx 20\sigma$) with various wettability parameters at the same temperature as ours. Although the uncertainty in the present results is large for small CAs, the present results were reasonably close to those obtained by the mechanical approach using a LJ fluid on the simplest structure-less wall modeled by a one-dimensional potential function, where τ_ℓ was around -3×10^{-12} N. This indicates that the line tension, indeed, appeared as a result of the crossing of the three interfaces and also that a consistent value can be evaluated in either the two quasi-2D systems of Bey *et al.*[8] and the approach used in this work without the CL curvature. Note this assumes the CA controlled by the wettability parameter is the same and a sufficiently large bulk liquid volume exists in the droplet. Regarding the uncertainty, with the present method, with the increase in η, both $w_{SL} - w_{SV}$ and s_{SL} become large and the resulting error of $(w_{SL} - w_{SV} - \gamma_{LV})s_{SL}$ and W_{drop} in the RHS of Eq. (26) become large. Due to this limitation, the increase in τ_ℓ with the decrease in θ_{CL} up to a positive value indicated in the mechanical result[8] is not obvious. Meanwhile, the geometric approach overall has large error bars, which is inevitable upon the fitting procedure of $\cos\theta_{LT}$–κ to obtain τ_ℓ in Eq. (31) (see Fig. 9 in Appendix B).

We finish with a discussion of error. For the geometric method, it is advantageous because of its simplicity, but also because of its simplicity, it gives neither mechanical nor thermodynamic explicit insights about line tension. In addition, as indicated by Ravipati *et al.*,[42] an accurate calculation of the CA from the density distribution may need long averaging times. Regarding the present thermodynamic approach, in addition to the problem of assuming the liquid volume to be constant for wettable cases mentioned above, the error $\delta\tau_\ell$ of τ_ℓ depends on the error δA_c of A_c with

$$\frac{\delta\tau_\ell}{\delta A_c} \approx \frac{\mathrm{d}\tau_\ell}{\mathrm{d}A_c} = \gamma_{LV}\frac{\sqrt{\pi} - \sqrt{\theta_{CL} - \cos\theta_{CL}\,\sin\theta_{CL}}}{2\sqrt{A_c}}, \quad (33)$$

and this monotonically increases with the decrease in θ_{CL}. Therefore, the error increase for the estimation of τ_ℓ is basically inevitable for small θ_{CL}. It is also seen from Eq. (33) that the relative error $\frac{\delta\tau_\ell}{\delta A_c}$ is proportional to $A_c^{-1/2}$, and it should decrease with the increase in A_c, meaning that it can be reduced by using a larger system size. Regarding the computational cost, both the mechanical and present thermodynamic methods do not need local stress calculation, which is computationally demanding. A longer time averaging of the ordinary equilibrium MD calculation would reduce the error for both.

IV. CONCLUDING REMARKS

In this study, we reviewed the mechanical interpretation of Young's equation where the line tension is obtained from the microscopic force balance. We then showed a thermodynamics interpretation of the line tension as the free energy per CL length, obtained from the difference between a quasi-2D hemi-cylindrical droplet on a solid surface and a cylindrical droplet with the same volume. Using this concept, we obtained the value of the line tension τ_ℓ through MD simulations of a quasi-static detachment process of a quasi-2D droplet from a solid surface, an extension of the thermodynamic integration method used to calculate the SL and SV interfacial tensions individually. Through the comparison with the results obtained in a mechanical manner, it was shown that the present thermodynamic approach provided a novel way to obtain the line tension.

SUPPLEMENTARY MATERIAL

The supplementary material contains how to evaluate the average A_c of the droplet area A for various η values and its uncertainty δA_c used in Eq. (28).

ACKNOWLEDGMENTS

AUTHOR DECLARATIONS

Conflict of Interest

The authors have no conflicts to disclose.

Author Contributions

Minori Shintaku: Conceptualization (lead); Data curation (lead); Formal analysis (lead); Investigation (lead); Methodology (equal); Project administration (equal); Validation (lead); Visualization (lead); Writing – original draft (supporting); Writing – review & editing (supporting). **Haruki Oga**: Data curation (supporting); Formal analysis (supporting); Investigation (supporting); Methodology (supporting); Project administration (supporting); Supervision (equal); Validation (supporting); Visualization (supporting). **Hiroki Kusudo**: Conceptualization (supporting); Data curation (supporting); Formal analysis (supporting); Investigation (supporting); Methodology (supporting); Project administration (supporting); Supervision (equal); Validation (supporting); Visualization (supporting); Writing – review & editing (equal). **Edward R. Smith**: Conceptualization (supporting); Validation (equal); Writing – original draft (supporting); Writing – review & editing (equal). **Takeshi Omori**: Conceptualization (supporting); Data curation (supporting); Formal analysis (supporting); Funding acquisition (supporting); Investigation (supporting); Validation (supporting); Visualization (supporting); Writing – original draft (supporting); Writing – review & editing (equal). **Yasutaka Yamaguchi**: Conceptualization (lead); Data curation (supporting); Formal analysis (supporting); Funding acquisition (lead); Investigation (equal); Methodology (equal); Project administration (lead); Resources (lead); Software (supporting); Supervision (lead); Validation (equal); Visualization (supporting); Writing – original draft (lead); Writing – review & editing (equal).

DATA AVAILABILITY

The data that support the findings of this study are available from the corresponding author upon reasonable request.

APPENDIX A: STRESS DISTRIBUTION AND SURFACE NORMAL FORCE ON THE SOLID WALL

Figure 8 shows the distributions of the stress component τ_{zz} in the droplet and the pressure exerted on walls of $\eta = 0.2$, 0.4, and 0.65 at $T = 100$ K for quasi-2D systems. The local stress was obtained by the volume average (VA),[18,26,59] whereas the pressure exerted on the wall was calculated by directly time-averaging the local force on the wall. Considering that the droplets showed Brownian motion on the solid surface, the distributions were taken around the center of mass of the droplet with the bin sizes of $0.02 \times 0.02 \times 4.0$ nm^3 and 0.02×4.0 nm^2 for the VA and the wall, respectively.

The stress component τ_{zz} was homogeneous in the liquid and vapor bulk away from the interface and was inhomogeneous around the interfaces as well as around the CL. Meanwhile, the pressure value p_{wall} exerted on the wall was also constant at $p_L^{\text{bulk}} > 0$ around the SL interface and SV interface at $p_V^{\text{bulk}} \approx 0$ interfaces, while that was negative around the CL, i.e., the wall was pulled upward by the LV surface tension there. The constant values τ_{zz} in the liquid and vapor bulk corresponded to the constant value of $-p_{\text{wall}}$ at the SL and SV interfaces, respectively, and we evaluated the droplet radius R from these values through the Young–Laplace equation [Eq. (S3) of the supplementary material] with $p_{\text{int}} = p_L^{\text{bulk}}$ and $p_{\text{ext}} = p_V^{\text{bulk}}$ in this study.

APPENDIX B: LINE TENSION DETERMINED FROM THE SIZE DEPENDENCE OF 3D-DROPLETS

Figure 9 shows the schematic of the calculation of line tension from the size dependence of $\cos\theta_{\text{LT}}$ on the CL curvature κ based on Eq. (3) with the data $\eta = 0.4$, 0.45, and 0.5 for three-dimensional droplets, where equilibrium droplets consisting of N_f fluid particles of 5832, 6859, 8000, 9261, 10648, and 12167 as well as for the quasi-2D droplets in the main text were used.[9,10] We obtained the CAs of three-dimensional hemi-spherical (cap-shaped) droplets from the time-averaged axisymmetric density distribution around the center of mass of the droplet.[60] More concretely, the contact angle θ_{LT} was defined as the angle between the LV interface and the solid–fluid
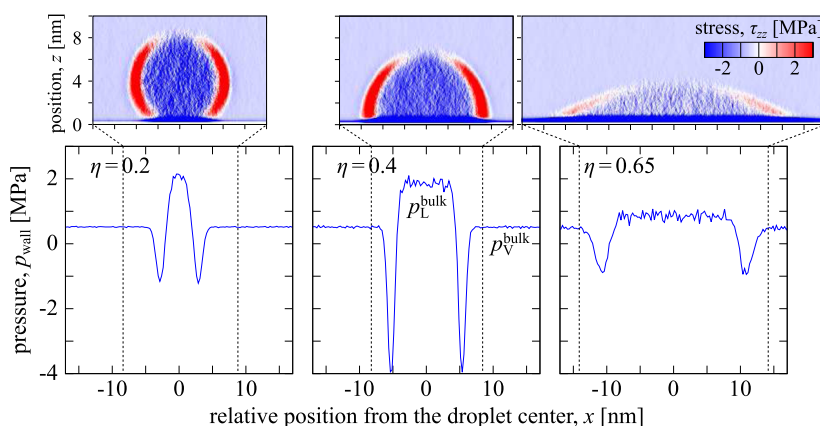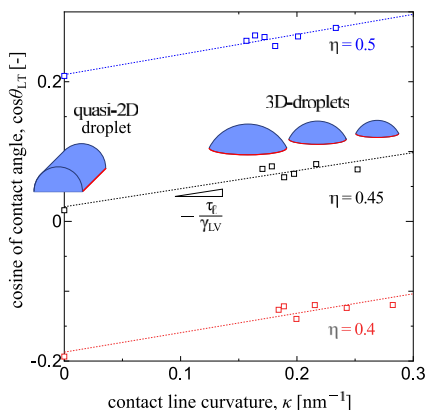
FIG. 8. Distributions of the (top) stress component τ_{zz} in the fluid and (bottom) pressure p_{wall} exerted on walls of $\eta = 0.2$, 0.4, and 0.65 at $T = 100$ K.

FIG. 9. Schematic of the calculation of line tension from the size dependence of the contact angle θ_{LT} based on Eq. (3) (with the data of $\eta = 0.4$, 0.45, and 0.5 at $T = 100$ K).

interface plane, where θ_{LT} was obtained by fitting a density contour at $\rho = 400$ kg/m^3 at the LV interface away from the solid with a spherical surface with a constant curvature.[26,29] Meanwhile, the solid–fluid interface position was defined as the limit position nearest to the solid that the fluid molecule could reach.[29] From the geometric information of the hemi-spherical droplet radius R and the contact angle θ_{LT}, we evaluated the CL curvature $\kappa = 1/R \sin \theta_{LT}$. By fitting the data with a straight line including the CAs of the quasi-2D droplets as θ_{LT} at $\kappa = 0$, we obtained the values of τ_ℓ for various solid–fluid interaction parameters η in Fig. 7. As indicated in this figure, the fitting includes points of three-dimensional hemi-spherical droplets with κ (= $1/r$ with r being the CL radius) around 0.2 nm^{-1} and a point of a quasi-two-dimensional hemi-cylindrical droplet with $\kappa = 0$, and the resulting uncertainty becomes inevitably large for this geometric approach.

REFERENCES

[1] T. Young, Philos. Trans. R. Soc. London **95**, 65 (1805).

[2] L. Gao and T. J. McCarthy, Langmuir **25**, 14105 (2009).

[3] J. W. Gibbs, *The Scientific Papers of J. Willard Gibbs, Thermodynamics* (Dover, 1961), Vol.1, pp. 557–571.

[4] S. Ono and S. Kondo, "Molecular theory of surface tension in liquids," in *Encyclopedia of Physics/Handbuch der Physik* (Springer, Berlin, 1960), Vol. 10, pp. 134–280.

[5] J. S. Rowlinson and B. Widom, *Molecular Theory of Capillarity* (Dover, 1982).

[6] J. S. Rowlinson, *Cohesion: A Scientific History of Intermolecular Forces* (Cambridge University Press, 2002).

[7] L. Boruvka and A. W. Neumann, J. Chem. Phys. **66**, 5464 (1977).

[8] R. Bey, B. Coasne, and C. Picard, J. Chem. Phys. **152**, 094707 (2020).

[9] T. Ingebrigtsen and S. Toxvaerd, J. Phys. Chem. C **111**, 8518 (2007).

[10] A. Marchand, J. H. Weijs, J. H. Snoeijer, and B. Andreotti, Am. J. Phys. **79**, 999 (2011).

[11] H. Teshima, H. Kusudo, C. Bistafa, and Y. Yamaguchi, Nanoscale **14**, 2446 (2022).

[12] Y. Heima, H. Teshima, and K. Takahashi, J. Phys. Chem. Lett. **14**, 3561 (2023).

[13] J. G. Kirkwood and F. P. Buff, J. Chem. Phys. **17**, 338 (1949).

[14] J. H. Irving and J. G. Kirkwood, J. Chem. Phys. **18**, 817 (1950).

[15] R. C. Tolman, J. Chem. Phys. **17**, 333 (1949).

[16] G. Bakker, *Kapillarität und Oberflächenspannung* (Wien-Harms, 1928), Vol. 6.

[17] M. P. Allen and D. J. Tildesley, *Computer Simulation of Liquids* (Oxford University Press, 1987).

[18] K. Shi, E. R. Smith, E. E. Santiso, and K. E. Gubbins, J. Chem. Phys. **158**, 040901 (2023).

[19] M. J. P. Nijmeijer, J. M. J. van Leeuwen, and J. M. J. Leeuwen, J. Phys. A: Math. Gen. **23**, 4211 (1990).

[20] M. J. P. Nijmeijer, C. Bruin, A. F. Bakker, and J. M. J. van Leeuwen, Phys. Rev. A **42**, 6052 (1990).

[21] J. Z. Tang and J. G. Harris, J. Chem. Phys. **103**, 8201 (1995).

[22] G. J. Gloor, G. Jackson, F. J. Blas, and E. De Miguel, J. Chem. Phys. **123**, 134703 (2005).

[23] S. K. Das and K. Binder, Europhys. Lett. **92**, 26006 (2010).

[24] J. H. Weijs, A. Marchand, B. Andreotti, D. Lohse, and J. H. Snoeijer, Phys. Fluids **23**, 022001 (2011).

[25] D. Seveno, T. D. Blake, and J. de Coninck, Phys. Rev. Lett. **111**, 096101 (2013).

[26] S. Nishida, D. Surblys, Y. Yamaguchi, K. Kuroda, M. Kagawa, T. Nakajima, and H. Fujimura, J. Chem. Phys. **140**, 074707 (2014).

[27] Y. Imaizumi, T. Omori, H. Kusudo, C. Bistafa, and Y. Yamaguchi, J. Chem. Phys. **153**, 034701 (2020); arXiv: 2004.14248.

[28] D. Surblys, Y. Yamaguchi, K. Kuroda, M. Kagawa, T. Nakajima, and H. Fujimura, J. Chem. Phys. **140**, 034505 (2014).

[29] Y. Yamaguchi, H. Kusudo, D. Surblys, T. Omori, and G. Kikugawa, J. Chem. Phys. **150**, 044701 (2019).

[30] H. Kusudo, T. Omori, and Y. Yamaguchi, J. Chem. Phys. **151**, 154501 (2019).

[31] F. Leroy, D. J. V. A. Dos Santos, and F. Müller-Plathe, Macromol. Rapid Commun. **30**, 864 (2009).

[32] F. Leroy and F. Müller-Plathe, J. Chem. Phys. **133**, 044110 (2010).

[33] F. Leroy and F. Müller-Plathe, Langmuir **31**, 8335 (2015).

[34] M. Kanduč, J. Chem. Phys. **147**, 174701 (2017).

[35] D. Surblys, F. Leroy, Y. Yamaguchi, and F. Müller-Plathe, J. Chem. Phys. **148**, 134707 (2018).

[36] C. Bistafa, D. Surblys, H. Kusudo, and Y. Yamaguchi, J. Chem. Phys. **155**, 064703 (2021).

[37] E. M. Grzelak and J. R. Errington, J. Chem. Phys. **128**, 014710 (2008).

[38] G. V. Lau, I. J. Ford, P. A. Hunt, E. A. Müller, and G. Jackson, J. Chem. Phys. **142**, 114701 (2015).

[39] V. Kumar and J. R. Errington, Phys. Procedia **53**, 44 (2014).

[40] V. R. Ardham, G. Deichmann, N. F. van der Vegt, and F. Leroy, J. Chem. Phys. **143**, 243135 (2015).

[41] H. Jiang, F. Müller-Plathe, and A. Z. Panagiotopoulos, J. Chem. Phys. **147**, 084708 (2017).

[42] S. Ravipati, B. Aymard, S. Kalliadasis, and A. Galindo, J. Chem. Phys. **148**, 164704 (2018).

[43] T. Omori, Y. Kobayashi, Y. Yamaguchi, and T. Kajishima, Soft Matter **15**, 3923 (2019).

[44] K. Watanabe, H. Kusudo, C. Bistafa, T. Omori, and Y. Yamaguchi, J. Chem. Phys. **156**, 054701 (2022).

[45] M. Shao, J. Wang, and X. Zhou, Sci. Rep. **5**, 1 (2015).

[46] H. Kusudo, T. Omori, and Y. Yamaguchi, J. Chem. Phys. **155**, 184103 (2021).

[47] M. V. Berry, "Liquid surfaces," in *Surface Science (Trieste, 16 Jan.–10 April 1974), Proceedings Series* (International Atomic Energy Agency, Vienna, 1975), Vol. 1, pp. 291–327.

[48] D. Schofield and J. R. Henderson, Proc. R. Soc. A **379**, 231 (1982).

[49] T. Saito, E. Shoji, M. Kubo, T. Tsukada, G. Kikugawa, and D. Surblys, J. Chem. Phys. **154**, 114703 (2021).

[50] J. Q. Broughton and G. H. Gilmer, J. Chem. Phys. **84**, 5759 (1986).

[51] R. L. Davidchack and B. B. Laird, Phys. Rev. Lett. **85**, 4751 (2000).

[52] R. L. Davidchack and B. B. Laird, J. Chem. Phys. **118**, 7651 (2003).

[53] R. Shuttleworth, Proc. Phys. Soc. A **63**, 444 (1950).

[54] B. Andreotti and J. H. Snoeijer, Europhys. Lett. **113**, 66001 (2016).

[55] H. Yaguchi, T. Yano, S. Fujikawa, and J. Fluid, J. Fluid Sci. Technol. **5**, 180 (2010).

[56] E. A. Mastny and J. J. de Pablo, J. Chem. Phys. **127**, 104504 (2007).

[57] A. Marmur, J. Colloid Interface Sci. **186**, 462 (1997).

[58] C. Herrero, T. Omori, Y. Yamaguchi, and L. Joly, J. Chem. Phys. **151**, 041103 (2019).

[59] K. Shi, E. E. Santiso, and K. E. Gubbins, J. Chem. Phys. **154**, 084502 (2021).

[60] D. Surblys, Y. Yamaguchi, K. Kuroda, T. Nakajima, and H. Fujimura, J. Chem. Phys. **135**, 014703 (2011).

21 October 2024 15:20:43